PNAS

Supporting Information for

Correlating histone acetylation with nucleosome core particle dynamics and function.

Tae Hun Kim*,+, Michael L. Nosella+, Nicolas Bolik-Coulon, Robert W. Harkness, Shuya Kate Huang, and Lewis E. Kay*

+Both authors contributed equally.

*Corresponding authors:
Tae Hun Kim (txk560@case.edu), Lewis E. Kay (kay@pound.med.utoronto.ca)

This PDF file includes:

Supporting Information Text
Figures S1 to S12
SI References

Supporting Information Text

Materials & Methods

Sample preparation
Histones

The four histone genes were subcloned into pET21b vectors for overexpression of histone proteins. In the case of H2B, a hexa-histidine tag followed by a TEV protease cleavage site was inserted at the N-terminus, whereas other histones were expressed as tagless proteins. A mutant (C110S) H3 was prepared and used in all studies to prevent the formation of disulfide bonds. To increase the expression yield of H4 and H2B, an isoleucine residue was inserted after the first methionine and the TEV cleavage site, respectively. Histones H2A, H2B, H3, H4 (*Drosophila melanogaster*), including WT and mutant forms, were expressed in *E. coli* as previously published (1).

After transforming the histone plasmids into *E. coli* BL21(DE3)-RIPL-CodonPlus, the cells were cultured at 37 °C until an OD600 of 0.8 was reached, at which point 1 mM IPTG was added. The cultures were subsequently allowed to incubate overnight at 37 °C. For expression of histone H4, the cells were induced for 5 hours instead of overnight. Histones labeled with NMR-active nuclei were expressed in M9 minimal media (6 g/L Na_2HPO_4, 3 g/L KH_2PO_4, 1 g/L NaCl, 1 g/L NH_4Cl at pH or pD 7.4) supplemented with 2 mM $MgSO_4$, 0.1 mM $CaCl_2$, 10 mg of biotin and thiamine, and 3 g of glucose. Uniformly ^{2}H, ^{13}C, ^{15}N-labeled histones were produced by cultivating the cells in M9 media prepared with $^{15}NH_4Cl$ (Cambridge Isotope Laboratories), $^{13}C_6$,$^{2}H_7$-glucose (Cambridge Isotope Laboratories) and D_2O (Cambridge Isotope Laboratories). For producing deuterated, ^{15}N, ILV-labeled histones, the cells were cultivated in deuterated M9 minimal media containing $^{15}NH_4Cl$, $^{12}C_6$,$^{2}H_7$-glucose and methyl precursors (60 mg/L of ^{13}C-methyl, 3,3-^{2}H, α-ketobutyric acid, and 80 mg/L of 3-methyl-^{13}C, 3,4,4,4-^{2}H, α-ketoisovaleric acid) were added to the culture 1 hour prior to induction. After harvesting, cell pellets were processed for histone purification or stored at -20 °C.

Purification of the tagless histones (H2A, H3, and H4) was achieved by resuspending the cell pellets in wash buffer with Triton X-100 (50 mM Tris, 100 mM NaCl, 1% (v/v) Triton X-100, pH 7.5). Cells were lysed by sonication (2 seconds on and 2 seconds off for 10 min, 30% power level, Q Sonica Q500) on ice. After centrifugation (18,000 g for 30 min), pellets were resuspended in wash buffer without Triton X-100 (50 mM Tris, 100 mM NaCl, pH 7.5) and sonicated on ice as above. After centrifugation (18,000 g for 30 min), the pellets were resuspended in unfolding buffer (20 mM Tris, 6 M GdnHCl, pH 7.5) and sonicated as above. The lysates were clarified by centrifugation (18,000 g for 30 min) and dialyzed twice (1 L each) against urea buffer (7 M urea, 50 mM sodium phosphate, 1 mM EDTA, 50 mM NaCl, pH 7.4). For preparing the urea buffer, 2 L of 7 M urea solution was treated with ~50 g of Amberlite beads (Millipore-Sigma) for 1 hour at room temperature to limit carbamoylation of lysine sidechains. Dialyzed histone samples were applied to a 5 mL HiTrap SP XL column (Cytiva) and purified over a NaCl gradient from 50 to 1000 mM using SP column buffer A (7 M urea, 50 mM sodium phosphate, 50 mM NaCl, pH 7.4) and SP column buffer B (7 M urea, 50 mM sodium phosphate, 1 M NaCl, pH 7.4). After dialyzing purified histone fractions against deionized water twice (5 L each), the purified histone samples were lyophilized and stored at -20 °C.

Purification of His-tagged H2B involved resuspension of the cell pellets in wash buffer (50 mM Tris, 100 mM NaCl, 1% [v/v] Triton X-100, pH 7.5) and lysing by sonication (2 seconds on and 2 seconds off for 10 min, 30% power level) on ice. After centrifugation (18,000 g for 30 min), the pellets were resuspended in denaturing buffer (6 M GdnHCl, 20 mM sodium phosphate, 500 mM NaCl, 20 mM imidazole, pH 7.5). The resuspended lysate was sonicated (2 seconds on and 2 seconds off for 10 min, 30% power level) on ice. After removing cell debris by centrifuging the lysate at 12,000 g for 20 min, the supernatant was applied to Ni-NTA resin (Cytiva) pre-equilibrated with denaturing buffer. The Ni-NTA resin was washed with 10 column volumes (CVs) of denaturing buffer to remove proteins non-specifically bound to the Ni-NTA resin. His-tagged H2B was eluted using elution buffer (6 M GdnHCl, 20 mM sodium phosphate, 500 mM NaCl, 300 mM imidazole, pH 7.5) and was buffer-exchanged to cold TEV cleavage buffer (20 mM sodium phosphate, 500 mM Arg-HCl, 0.5 M NaCl, 2 mM DTT), using a fast dilution method, for overnight cleavage of the His-tag with TEV protease at 4°C. The cleaved His-tag and TEV protease were removed by

applying the TEV cleavage reaction mixture (supplemented with 30 mM of imidazole) to Ni-NTA. After dialyzing the purified H2B against deionized water twice (5 L each time), the H2B sample was lyophilized for long-term storage at -20°C.

601 DNA

A pUC19 plasmid DNA carrying ~30 copies of 153-bp 601 DNA was transformed into *E. coli* (BL21DE3) and grown on LB-agar containing 100 µg/mL of ampicillin overnight at 37 °C. A single colony was picked and grown in 5 mL of Terrific Broth containing 100 µg/mL ampicillin, 4 mL/L glycerol, and 7 mM $MgSO_4$ at 37 °C. After reaching an OD600 of ~2.0, the 5 mL culture was transferred to 100 mL of Terrific Broth (Wisent Bioproducts) containing 100 µg/mL ampicillin, 4 mL/L glycerol, and 7 mM $MgSO_4$ and grown to an OD600 of ~1.5 at 37 °C. The 100 mL *E. coli* culture was transferred to 1 L of Terrific Broth containing 100 µg/mL ampicillin, 4 mL/L glycerol, and 7 mM $MgSO_4$ and cultured overnight at 37 °C. Plasmid DNA from the 1 L of Terrific Broth culture was extracted using a Plasmid Giga kit (QIAGEN). The purified plasmid DNA was digested with EcoRV (NEB) in NEB3 buffer (50 mM Tris, 100 mM NaCl, 10 mM $MgCl_2$, pH7.9) overnight at 37 °C. The digested DNA was purified using a 5 mL HiTrap DEAE Sepharose FF column (Cytiva). The 153-bp 601 DNA bound the DEAE column (Cytiva) whereas most of the backbone DNA was found in the flow-through. The bound 601 DNA was eluted using a NaCl gradient from 0 to 1 M over 75 mL. The eluted DNA fraction was applied to a Superdex 200 HiLoad 26/600 column (Cytiva) pre-equilibrated in RB high buffer (10 mM Tris, 2 M KCl, 1 mM EDTA, pH 7.4) to remove residual backbone DNA and 12-bp linker DNA. The purified 153-bp 601 DNA was concentrated using an Amicon Ultra-15 centrifugal concentrator with 10 kDa cutoff and stored at 4 or -20 °C.

p300

The construct for expressing the catalytic domain of human p300 was a generous gift from Dr. Michael Rosen at UT Southwestern Medical Center. *E. coli* cells (BL21(DE3)-RIPL-CodonPlus) transformed with this construct, which encodes the catalytic domain of p300 (1287-1664) and the deacetylase SIR2 (87-562), were grown to an OD600 of 0.6 in Terrific Broth containing 100 µg/mL ampicillin and 25 µg/mL chloramphenicol and induced with 1 mM IPTG overnight at 18°C. After harvesting the cells by centrifugation, the pellets were resuspended in lysis buffer (50 mM HEPES, 1 M NaCl, 10 mM imidazole, 2 mM β-mercaptoethanol, 10% [w/v] glycerol, 1 mM benzamidine, one SigmaFAST protease inhibitor cocktail EDTA-free tablet/100 mL, 0.5% of Triton X-100, pH 7.0) and lysed by sonication using a 2 mm probe set to 30% power output, 50% duty cycle, over 10 min. The supernatant obtained after centrifuging the lysate for 30 minutes at 18,000 g was applied to a 5 mL HiTrap Ni-NTA column (Cytiva) pre-equilibrated with the lysis buffer. After loading the lysate onto a 5 mL HiTrap Ni-NTA column (Cytiva), a gradient of imidazole from 25 mM to 300 mM over 150 mL was applied using wash buffer (50 mM HEPES, 1 M NaCl, 25 mM imidazole, 2 mM β-mercaptoethanol, 10% [v/v] glycerol, 1 mM benzamidine, 0.5% of Triton X-100, pH 7.0) and elution buffer (50 mM HEPES, 1 M NaCl, 300 mM imidazole, 2 mM β-mercaptoethanol, 10% [v/v] glycerol, 1 mM benzamidine, 0.5% of Triton X-100, pH 7.0). After collecting the fractions containing p300, Triton X-100 was removed by stirring with Bio-Beads SM-2 (Bio-rad). The hexa-histidine tag was cleaved by the addition of TEV protease overnight at 4 °C during dialysis against 20 mM Tris, 1 mM DTT, pH 8. The dialyzed sample was further purified using a MonoQ 5/50 column (GE Healthcare) by applying a NaCl gradient from 50 mM to 600 mM using ion exchange buffer A (20 mM Tris, 1 mM DTT, pH 8) and buffer B (20 mM Tris, 1 M NaCl, 1 mM DTT, pH 8). A final purification was performed using a Superdex 200 26/60 size exclusion column (Cytiva) pre-equilibrated in gel-filtration buffer (20 mM Tris, pH 8, 150 mM NaCl, 10% [v/v] glycerol, 1 mM DTT). After testing the HAT activity of the purified p300 on histones, aliquots were frozen in liquid N_2 and stored at -80 °C.

Ligase 3

The full-length, α-splice variant of *H. sapiens* DNA ligase 3 (LIG3) containing the C-terminal BRCA1 C-terminal homology domain (BRCT) was expressed and purified from *E. coli* as previously described (2), with some variations. Briefly, cDNA containing the LIG3α coding sequence was inserted in frame with an N-terminal hexahistidine-SUMO tag in a pET-SUMO vector construct (Thermo Fisher) via Gibson Assembly (New England Biolabs). Expression of the construct in *E. coli* BL21 (DE3) C41 cells was performed exactly as described (2). Bacteria were harvested and

resuspended in lysis buffer: 25 mM Tris, 10%v/v glycerol, 25 mM imidazole, 250 mM NaCl, pH 7.5. Small amounts of powdered DNase I (Roche) and lysozyme (BioBasic) were added to aid in DNA fragmentation and cell wall disruption, respectively. Cells were lysed on ice by sonication using a 2 mm probe set to 30% power output, with 50% duty cycles over 4min. periods. After clarification by centrifugation, the lysate was loaded onto a nickel-NTA gravity column (GE Healthcare) with 10 mL bed volume pre-equilibrated in the same lysis buffer as above. Bound proteins were eluted in steps of elution buffer containing 25 mM Tris, 10%[v/v] glycerol, 250 mM NaCl, 2 mM β-mercaptoethanol, pH 7.5 and 100 mM or 250 mM imidazole. Fractions containing SUMO-tagged LIG3, as verified by SDS-PAGE analysis, were dialyzed into 25mM Tris, 500 mM NaCl, 2 mM β-mercaptoethanol, 0.5 mM benzamidine, pH 7.5 overnight at 4°C. The SUMO tag was cleaved by addition of SUMO protease Ulp (Thermo Fisher). The dialyzed sample was then re-purified on the nickel-NTA column using the same procedure as above, except the tag-less LIG3 was isolated in the flow-through and low-imidazole wash fractions, which were subsequently concentrated using an Amicon Ultra-15 centrifugal concentrator unit (Millipore) equipped with a 50 kDa molecular weight-cutoff membrane. The concentrated sample was diluted into 25 mM HEPES, 10%[v/v] glycerol, 300 mM NaCl, 0.5 mM EDTA, 2.5 mM β-mercaptoethanol, pH 7.5 and injected onto a 5 mL HiTrap Blue column (GE Healthcare) pre-equilibrated in the same buffer using a peristaltic pump. Proteins were eluted over a linear gradient from 300 mM to 2 M NaCl. Fractions containing LIG3 were pooled and concentrated for injection onto a Superdex 200 26/60 size exclusion column (Pharmacia) pre-equilibrated in 25 mM Tris, 1 M NaCl, 0.5 mM EDTA, 2 mM DTT, pH 7.5. The purified LIG3 was then dialyzed into storage buffer (25 mM Tris, 500 mM NaCl, 1 mM TCEP, 0.5 mM EDTA, pH 7.5), concentrated and stored at -80°C until later use.

Metagenome-derived alkaline phosphatase (mAP)

The expression and purification of mAP were performed as described (3). The codon-optimized ORF of mAP (GeneBank accession number of GQ250428) was subcloned into pET-21a in frame with a C-terminal hexa-histidine tag. *E. coli* (BL21DE3-RIPL-CodonPlus) cells were transformed with this construct and cultured in LB containing 100 µg/mL ampicillin at 37°C until an OD600 of 0.4-0.6 was attained. Overexpression of mAP was induced with 0.5 mM IPTG at 18°C for 18 hours. After harvesting, the cell pellet was resuspended in periplasmic buffer (200 mM Tris–HCl, 20% [w/v] sucrose, 1 mM EDTA, lysozyme at pH 7.5). After incubating the resuspended cells on ice for 5 minutes, osmotic shock was achieved by quickly adding an equal volume of cold water. To obtain the periplasmic fraction, the cell suspension was centrifuged at 12,000 g for 20 minutes. The supernatant was applied to Ni-NTA resin pre-equilibrated in wash buffer (25 mM Tris, 250 mM NaCl, 20 mM imidazole, 10%[v/v] glycerol, one SigmaFAST protease inhibitor cocktail EDTA-free tablet/100 mL, 2 mM β-mercaptoethanol, pH 7.5). The Ni-NTA resin was washed with 3 CVs of wash buffer, followed by 3 CVs of wash buffer with 100 mM imidazole added. The mAP was eluted with 5 CVs of elution buffer (25 mM Tris, 250 mM NaCl, 250 mM imidazole, 10% glycerol, 2 mM β-mercaptoethanol, pH 7.5). The eluted mAP fractions were concentrated and applied to a HiLoad 16/600 Superdex 200 column (Cytiva) pre-equilibrated in gel-filtration buffer (25 mM Tris, 500 mM NaCl, 0.5 mM EDTA, 2 mM DTT, pH 7.5). After concentrating the mAP-containing fractions from size-exclusion chromatography, aliquots of mAP were flash frozen with liquid N_2 and stored at -80 °C until later use.

Nt.BsmAI

We used BsmAI with an R221D mutation (Nt.BsmAI) (4) to introduce a single-strand nick in 153-bp 601 DNA. The DNA sequence below shows where the nick is located '^'.

5´ATCCTGGAGAATCCCGGTGCCGAGGCCGCTCAATTGGTCGTAGACAGCTCTAGCACCGCT
TAAACGCACGTACGCGCTGTCCCCCGCGTTTTAACCGCCAAGGGGATTACTCCCTAGTCTC
C^AGGCACGTGTCAGATATATACATCCTGTGAT3´

To co-express Nt.BsmAI, both His_6-SUMO-Nt.BsmAI and BsmAI methyltransferase (bsmAIM) were subcloned into a pCOLADuet-1 vector. Co-expression of both genes was necessary as even a minuscule amount of Nt.BsmAI activity was lethal to *E. coli*. (Note that methylation by bsmAI methyltransferase protects against BsmAI activity). For expression, *E. coli* (BL21DE3-RIPL-

CodonPlus) cells transformed with the plasmid DNA containing His_6-SUMO-Nt.BsmAI and BsmAI methyltransferase were grown to reach an OD600 of 0.6 in LB at 37°C and induced with 0.3 mM IPTG overnight at 18 °C. After harvesting the cells, cell pellets resuspended in lysis buffer (25 mM Tris, 500 mM NaCl, 2 mM β-mercaptoethanol, 20 mM imidazole, pH 7.5) were lysed by sonication (cycle of 2 seconds on and 2 seconds off for 10 minutes at 30% power). The lysate fraction obtained after centrifugation (12,000 g for 30 min) was applied to a Ni-NTA resin pre-equilibrated with lysis buffer. The Ni-NTA resin was washed with ~10 CVs of lysis buffer. His_6-SUMO-Nt.BsmAI was eluted with elution buffer (25 mM Tris, 500 mM NaCl, 2 mM β-mercaptoethanol, 300 mM imidazole, pH 7.5) and incubated with Ulp protease during dialysis against dialysis buffer (25 mM Tris, 250 mM NaCl, 2 mM β-mercaptoethanol, pH 7.5). After supplementing the dialyzed sample with 20 mM imidazole, the Ulp protease reaction mixture was applied to the Ni-NTA column to separate His_6-SUMO and Ulp protease from Nt.BsmAI. The Nt.BsmAI fraction was concentrated and applied to a Superdex 200 HiLoad 16/600 column (Cytiva) pre-equilibrated in gel-filtration buffer (25 mM Tris, 300 mM NaCl, 2 mM DTT, pH 8.0). The purest fractions containing Nt.BsmAI were pooled together, concentrated, and supplemented with 20 % glycerol for long-term storage at -80 °C.

Preparation of acetylated histones

Acetylation of purified histones was performed by incubating 50 μM of purified histones with 0.5 - 1 μM of p300 and 1 mM acetyl-coenzyme A in acetylation buffer (25 mM Tris, 2 mM DTT, pH 7.5) overnight at room temperature. In the case of H2B, 0.4 mM of acetyl-coenzyme A was used to limit the number of acetylation sites to eight, as reconstructing the NCP with maximally-acetylated H2B resulted in a heterogeneous population of NCP species as assessed by native PAGE. After confirming the number of acetylations by mass spectrometry, the acetylation reactions were quenched by adding GdnHCl to 4 M. To remove p300, the acetylation reaction mixtures were concentrated and applied to a Superdex 200 HiLoad 16/600 column (Cytiva) pre-equilibrated in 10 mM Tris, 6 M GdnHCl, 2 mM DTT, pH 7.5. Pure fractions of acetylated histones were concentrated and stored at -20 °C until later use.

Preparation of H2A-H2B dimers and H3-H4 tetramers

For samples involving acetylated H2B or comprising more than one acetylated histone we have found it necessary to mix H2A-H2B dimers with H3-H4 tetramers, as discussed previously (5); the procedure described below can be used to reconstitute NCPs with unmodified histones as well. For reconstituting H2A-H2B dimers, purified H2A and H2B dissolved in unfolding buffer (10 mM Tris, 6 M GdnHCl, pH 7.5) were mixed together in a 1:1 ratio at concentrations of 60-70 μM for each histone. The dimer sample was dialyzed against refolding buffer (10 mM Tris, 2 M NaCl (or KCl), 1 mM EDTA, pH 7.5) overnight at 4 °C. The dialysis was performed such that fresh refolding buffer was continuously added at the top of the dialysis chamber (plastic beaker; 2 liters at a flow rate of ~ 1.5mL/min), while buffer flowed out through a hole located at the 400 mL mark of the beaker. After dialysis, the reconstituted dimer was further purified using a Superdex 75 Increase 10/300 GL column (Cytiva) pre-equilibrated in refolding buffer at 4 °C. For reconstituting dimers with acetylated histones, refolding buffer with arginine (10 mM Tris, 1.5 M NaCl, 500 mM Arg-HCl, 1 mM EDTA, pH 7.5) was used instead. Unmodified and acetylated H3-H4 tetramers were prepared using the same procedure.

mAP reaction

To dephosphorylate the blunt ends of purified 601-DNA, the following reaction mixture was prepared: 25 mM Tris, 100 mM NaCl, 2 mM DTT, 1 mM $CaCl_2$, 3 μM 601-DNA. mAP was added to a final concentration of 500 nM to initiate the reaction, which was allowed to proceed overnight at 37 °C. The next day, mAP activity was confirmed using a ligation assay. Briefly, a 1 μL sample of the mAP reaction mixture was diluted into a 10 μL volume containing 1 mM ATP-Mg, 1 mM DTT, 25 mM Tris pH 7.5, and 40000 U of T4 DNA ligase (NEB) and allowed to incubate at 37 °C for 10 min. The products were resolved on a 1% agarose-TAE gel. In the event of complete removal of terminal phosphates, the 601-DNA would travel as a discrete band corresponding to ~153-bp, having not undergone concatenation in the presence of ligase.

The mAP reaction was quenched by submersion in boiling water for ~10 min. followed by rapid cooling on ice. The 601-DNA was purified from the other reaction components on a monoQ 5/50 anion exchange column, which was pre-equilibrated in 10 mM Tris, 0.1 mM EDTA, pH 8.0. DNA was eluted with a linear NaCl gradient spanning 0 to 1 M NaCl over 50 mL intervals. 601-DNA would typically elute at salt concentrations approaching ~600 mM. The purified DNA was then exchanged into water for subsequent nicking.

Nicking reaction

mAP-treated 601-DNA (dissolved in water) was diluted to a final concentration of 500 nM in a reaction mixture containing the following: 50 mM Tris, 300 mM NaCl, 10 mM $MgCl_2$, pH 8.7. Note that the described salt and pH conditions were specifically optimized to favor single-strand nicking activity over double-strand excision. Purified Nt.BsmAI was added to a final concentration of 100 nM to initiate the nicking reaction, which was allowed to proceed overnight at 37 °C. The next day, the reaction mixture was diluted to a final salt concentration of ~100 mM NaCl so that the DNA could be purified on the monoQ 5/50 column (Pharmacia) as described in the previous section. Nicking activity was confirmed by resolving small samples of the reaction mixture on native 6%-TBE polyacrylamide and 15% TBE-urea polyacrylamide gels (Invitrogen). The former confirmed that Nt.BsmAI did not catalyze double-strand breaks, which would lead to the accumulation of two DNA species migrating at ~31-base pairs (bp) and ~122-bp, while the latter confirmed the presence of a single-strand nick, which would give rise to three species migrating at ~31 nucleotides (nt), ~122 nt and ~153 nt (*i.e.*, the full length of the complementary, unnicked strand).

The purified, nicked 601-DNA was then exchanged into high salt refolding buffer (RB High: 10 mM Tris, 2 M KCl, 1 mM EDTA, pH 7.4) for NCP reconstitution. To prepare Alexa Fluor 647 (AF647)-labeled nicked 601-DNA for the ligation assays, the DNA would instead be exchanged into 25 mM Tris, 100 mM NaCl, pH 7.5 and mixed in a 1:1 ratio with a 5'-phosphorylated, 3′-AF647-labeled oligonucleotide (IDT) possessing the same sequence as the final 31 nucleotides of 601-DNA. This mixture was heated to 95°C in a PCR machine for 5 minutes before being allowed to cool to lab temperature on the bench. The nicked 601-DNA was then separated from the excess, dye-labeled 31 nt-oligonucleotide using a Superdex 200 10/300 column (Cytiva) pre-equilibrated in RB High. Incorporation of the dye-labeled oligonucleotide into the nicked 601-DNA was verified by native gel electrophoresis, wherein the fluorescent signal from the AF647 dye was detected in the DNA band corresponding to the full-length 601-DNA. Fractions containing the AF647-labeled, nicked 601-DNA (and the unlabeled, nicked 601-DNA) were concentrated in RB High and then mixed with unlabeled, nicked 601-DNA to yield a final dye concentration of 5 mol%, assuming that half of the nicked 601-DNA incorporated the AF647-labeled, 31 nt-oligonucleotide during the heat exchange step.

Preparation of nucleosome core particles (NCPs)

For preparing unmodified NCPs, H2A-H2B dimer, H3-H4 tetramer, and 153-bp 601 DNA were mixed together at a molar ratio of 2.2:1:1 (13.2:6:6 μM) in RB high buffer (10 mM Tris, 2 M KCl, 1 mM EDTA, pH 7.4). The NCPs were reconstituted by performing gradient dialysis from RB high buffer (400 mL) to RB low buffer (10 mM Tris, 0.15 M KCl, 1 mM EDTA, pH 7.4) at 4 °C by adding RB low buffer (2 L) at a flow rate of ~1.5 mL/min for 18 hours. The homogeneity and integrity of the NCP samples were validated by native gel electrophoresis (150 V for 60 min on ice). For preparing acetylated NCPs, the same procedure was used but with RB high buffer with arginine (10 mM Tris, 1.5 M KCl, 500 mM Arg-HCl, 1 mM EDTA, pH 7.5).

Ligation assay

Ligation reactions were prepared in 0.6mL thin-walled PCR tubes in a total volume of 30 μL per reaction. Each had the following composition: 25 mM Tris, pH 7.5, 112.5 mM NaCl, 37.5 mM KCl, 1 mM ATP-Mg, 1 mM DTT and 500 nM nicked-601 DNA-containing NCP (with varying acetylation patterns), of which 5% was labeled with AlexaFluor647 (AF647) on the 3′ end of the DNA. To initiate the reaction, LIG3 was added to a final concentration of 0.1 μM. An incubation series extending from 20 min. to 160 min. (unmodified NCP, or NCPs comprising H2A P116*, H2A

K73Q, K74Q P116*, acetylated H2A, acetylated H2B, acetylated H3, acetylated H4) or from 20 s to 180 s (NCPs with combinations of H2A and other acetylated histones) was recorded. Following each incubation period at 37 °C, a 5 μL volume of each reaction was quenched in 15 μL of loading buffer (8%[w/v] Ficoll PM-100 [Millipore-Sigma], 1.3x tris-borate-EDTA [TBE, Millipore-Sigma], 2.66 M urea) and then incubated at 95°C for 5min. After rapid cooling on ice, the samples were resolved on a 15% TBE-urea polyacrylamide gel (Invitrogen) pre-equilibrated in 0.5x TBE heated to 70 °C (180 V for 30 min). Ligated and unligated DNA species were measured via the fluorescence signal of the AF647 dye on a ChemiDoc MP imaging system (BioRad). For the stated conditions, exposure times of 15 s or longer were typically required. Gel images were analyzed in Fiji. Following background subtraction, raw band intensities were used to calculate ligation, which was quantified as the quotient of the ligated band intensity divided by the sum of the ligated band intensity and the unligated band intensity in the same lane.–Ligation rates (%Ligation/min) were subsequently calculated from the slope of the trendline fit to the ligation kinetics data obtained by linear regression.

Micrococcal nuclease (MNase) sensitivity assay

MNase reactions (10 μL) contained the following: 25 mM Tris, pH 7.5, 112.5 mM NaCl, 37.5 mM KCl, 2.5 mM $CaCl_2$, 500 nM nicked-601 DNA-containing NCP with varying acetylation patterns. The digestion was initiated by adding 1000 gel units of MNase directly as supplied by New England Biolabs. Following a 5 min. incubation period at 37°C, a 5 μL volume of each reaction was quenched in 15 μL of loading buffer, as in the ligation assays (see above) and resolved on 15 % TBE-urea gels (heated at 70 ºC) following a 5 min.-long 95°C incubation period. Gels were stained for ~5 min. with SYBR Gold (Thermo Fisher) diluted 1:10000 from the manufacturer-supplied dimethylsulfoxide stock solution into deionized water. Fragmented and intact DNA species were observed by measuring the SYBR Gold fluorescence signal on a ChemiDoc MP imaging system (BioRad).

Cryo-EM

Holey gold grids with approximately 2 μm holes were prepared in-house as previously described (6). Grids were glow-discharged in air for 15 s immediately prior to sample application. 3 μL of a 2 μM NCP sample in EM buffer (20 mM sodium phosphate, 100 mM NaCl, 0.1 mM EDTA, pH 7.4) was applied to each grid, followed by blotting from the gold side using a Leica EM GP2 plunge freezer (Leica Microsystems) for 0.5 s at 4 °C and approximately 95% humidity prior to freezing in liquid ethane. Samples were imaged with an FEI Tecnai F20 electron microscope equipped with a 200 keV field emission gun and applying a defocus range of 1 to 3 μm. Movies were acquired with a Gatan K2 Summit direct detection camera in counting mode using a calibrated magnification of 34,483×, corresponding to a pixel size of 1.45 Å. Exposures were collected at 0.5 s per frame for a total of 15 s, with an exposure of approximately 5.5 electrons/pixel/s and a total exposure of 40 electrons/$Å^2$. Movie frames were aligned using patch-based motion correction in cryoSPARC v.4 (7).

NMR spectroscopy

Samples

Reconstituted NCPs were buffer-exchanged into NMR buffer (20 mM sodium phosphate, 0.1 mM EDTA, 3% D_2O, pH 6.0) at typical concentrations between ~90 μM – 110 μM. A pair of NMR samples was prepared for each condition examined (*i.e.*, for each non-acetylated NCP and for each NCP containing a single acetylated histone), with one sample ^2H,^{13}C,^{15}N-labeled at one of the four histones (the others were uniformly ^2H-labeled), and a second sample where one histone is ILV-methyl labeled, as described above and in the main text, and deuterated at all other positions, with the other three histones perdeuterated. Note that in each acetylated NCP sample the single acetylated histone was always NMR active. Thus, 16 NCP samples were prepared in total: 8 samples with acetylation at each histone separately (both ^2H,^{13}C,^{15}N- and ILV-labeled) and an additional 8 samples, as the first 8, but with no acetylation.

Assignments of individual ^{13}C,^{15}N-labeled histones, both unmodified and acetylated, were obtained in order to quantify the position and extent of acetyl-group labeling. To this end

experiments was performed by dissolving histones in denaturing buffer (6 M urea, 25 mM MES, 3 % D_2O, pH 5.5) prior to recording spectra, to ensure that the acetylated histones (presumed of limited solubility since lysine residues are neutralized by the modification) would be soluble at protein concentrations of several hundred μM that were used.

NMR experiments

All NMR experiments were recorded using either 14.1 T or 18.8 T Bruker Avance III HD spectrometers, or with a 23.5 T Bruker Avance NEO spectrometer, each equipped with an *x*,*y*,*z* gradient TCI cryoprobe. All experiments on NCP samples were recorded at 37 °C. The integrity of each NCP sample was established by recording ^{1}H-^{15}N HSQC spectra using a gradient-enhanced HSQC experiment, 37 °C (18.8 T) (8), focusing on the histone tail regions, or via ^{1}H-^{13}C HMQC datasets, 37 °C (23.5 T) with water suppression achieved using a WATERGATE scheme (9).

Backbone and sidechain assignments of individual histones and of histone tails in NCPs

Backbone and side chain assignments of histones in denaturing buffer were obtained by recording a series of triple resonance experiments (HNCO, HN(CA)CO, HNCACB, HNN and C(CO)NH) at 25 °C, 18.8 T (10). An identical set of experiments (without C(CO)NH) was recorded for assignment of backbone nuclei of histone tails in NCPs, both for unmodified and acetylated samples, at 37 °C, 18.8 T, with the exception of the unmodified H3 tails for which detailed assignments were already available in the literature (11).

Assignment of NCP methyl groups

Assignments of ILV-methyl groups in the WT NCP construct are based on a previous study (12), while assignments in the acetylated variants could be easily transferred from the spectrum of the WT particle.

Measurement of dynamics in NCPs

(i) J(0) values of backbone amides

In order to obtain an exchange free measure of histone tail backbone mobility we have recorded ^{15}N{^{1}H}-heteronuclear NOEs, ^{15}N R_1 relaxation rates, and the relaxation rates of a series of four ^{15}N-^{1}H two spin terms, either in the presence or absence of ^{15}N and ^{1}H spin-lock fields, as described previously (13, 14). The four two spin terms are denoted by $2H_z'N_z'$, $2H_ZN_z'$, $2H_z'N_Z$, $2H_ZN_Z$ where the superscript prime indicates that a spin-lock field is applied to the spin in question, so that $A_Z' = A_Z\cos(\theta_A) + A_X\sin(\theta_A)$, and $\tan(\theta_A) = \frac{\omega_{1A}}{\Delta_A}$ with ω_{1A} and Δ_A the strengths of the *A* spin-lock field applied along the *x*-axis (rad/s) and the offset of the spin in question from the carrier position (rad/s), respectively. Expressing the linear combination of two-spin relaxation rates as

$$R_{\Sigma\rho} = \frac{1}{2}[R_{1\rho}(2H_z'N_Z) + R_{1\rho}(2H_ZN_z') - (R_{1\rho^2}(2H_z'N_z') + R_1(2H_ZN_Z)] \quad [1]$$

it follows that (13)

$$R_{dd} = R_{\Sigma\rho}/[\sin^2(\theta_H)\sin^2(\theta_N)] = \frac{d_{HN}^2}{8}(4J(0) - 3J(\omega_N) + 0.845J(0.87\omega_H)) \quad [2]$$

where $J(\omega)$ is a spectral density function evaluated at frequency ω, $d_{HN} = \frac{(\frac{\mu_0}{4\pi})\hbar\gamma_H\gamma_N}{r_{HN}^3}$, μ_0 is the vacuum permeability ($4\pi \times 10^{-7}\ N\ A^{-2}$), r_{HN} (1.02 Å) is the distance between ^{1}H and ^{15}N nuclei, $\hbar$ is Planck's constant h ($6.626 \times 10^{-34}\ J\ s$) divided by 2π, γ_H ($2.675 \times 10^{8}\ rad\ s^{-1}\ T^{-1}$) and γ_N ($-2.7116 \times 10^{7}\ rad\ s^{-1}\ T^{-1}$) are the gyromagnetic ratios for ^{1}H and ^{15}N, respectively. In the derivation of Eq. [2] it has been assumed that $J(\omega) \propto \frac{1}{\omega^2}$ (15).

The decay rates of $2H_z'N_z'$,$2H_ZN_z'$, $2H_z'N_Z$, $2H_ZN_Z$ were measured using previously published pulse schemes (13) with eight delays (5, 10, 15, 25, 35, 45, 55, 65) ms and spin lock powers of 2,000 Hz, and 13,200 Hz for ^{15}N and ^{1}H, respectively. Note that the delays used were identical for

all of these rate measurements. ^{15}N R_1 relaxation rates were obtained using the pulse scheme of Farrow *et al.* (16) with six delays (0.01, 0.1, 0.25, 0.4, 0.55, 0.7) s. ^{15}N{^{1}H}-heteronuclear NOEs were obtained from a pair of experiments recorded either with a pre-scan delay of 8 s followed by saturation for 6 s or a delay of 14 s, using the approach of Ferrage *et al.* (17). All NMR experiments were performed at 37 °C, 18.8 T.

Values for $J(\omega_N)$ and $J(0.87\omega_H)$ were calculated using ^{15}N{^{1}H}-heteronuclear NOEs, and ^{15}N R_1 rates, as described previously (13, 15), from which $J(0)$ values, reported in the paper, are obtained via Eq. [2]. In the case of isotropically tumbling proteins $J(0) = \frac{2}{5}S^2\tau_C$, with S^2 the square of an order parameter related to the amplitude of the amide bond vector motion and τ_C an effective tumbling time for the protein in question (18). Because the dynamics of intrinsically disordered proteins are extremely complex it is most straightforward to describe them in terms of the spectral density values themselves rather than interpreting these spectral densities further in terms of specific parameters, as is normally done for folded molecules.

(ii) Measuring methyl $S^2_{axis}\,\tau_C$ values

$S^2_{axis}\,\tau_C$ values were obtained as described previously (19) using an approach in which the sums (I_{SQ}) and differences (I_{3Q}) of single quantum methyl ^{1}H magnetization components are quantified. This was achieved using 14 delays (0.3, 0.5, 0.7, 1, 1.5, 2, 3, 4, 5, 6, 7, 8, 9, 10) ms with 16 or 32 and 96 scans for measuring I_{SQ} and I_{3Q}, respectively, for a total measurement time of between 3-4 days per dataset. All NMR experiments were recorded at 37 °C, 23.5 T with the exception of those measured on NCPs prepared with acetylated H2A, H2A P116*, and H2A K73Q, K74Q P116* where a lower field of 14.1 T was used, as exchange contributions were pervasive, and hence sensitivity was improved at 14.1 T relative to higher fields.

(iii) Methyl-TROSY based CPMG measurements

Methyl ^{1}H-^{13}C multiple quantum CPMG experiments were recorded at 37 °C, 14.1 T and 23.5 T using the pulse scheme of Korzhnev and coworkers (20). A constant relaxation time, T, of 10 ms was used, along with 11 ν_{CPMG} frequencies varying from 100 - 1200 Hz, with two duplicate points to estimate errors, for a net acquisition time of approximately 2 days/dataset. Dispersion profiles were generated as $R_{2,eff}$ *vs* ν_{CPMG} where $R_{2,eff} = -\frac{1}{T}\ln(\frac{I}{I_o})$ and I and I_o are the intensities of peaks recorded in spectra with and without the T delay, respectively. Dispersion data were analyzed using *ChemEx* software version 2022.0.0a0 (https://github.com/gbouvignies/ChemEx) assuming a two-state model of exchange. Profiles measured for V42b, L92δ1, L96δ2, V106b, L107a, L107b, V113b, L114δ2, L115δ1, and L115δ2 at both 14.1 T and 23.5 T were fitted globally and the errors in k_{ex} and the population of the minor state were calculated using 200 bootstrap simulations(21).

DLS studies

Sample preparation, diffusion measurements, and autocorrelation analysis

NCP stocks for DLS measurements were prepared in 20 mM sodium phosphate, 100 mM NaCl, 0.1 mM EDTA, pH 7.4 and diluted to obtain the desired total NCP concentration. The DLS buffer was filtered using a 0.2 µm syringe filter prior to use. Samples for DLS analysis were prepared using Eppendorf tubes that were evacuated of dust with compressed air. Prior to loading in the DLS plate wells, all samples were centrifuged at 17,500 rpm for 15 minutes to pellet any large aggregates or residual dust that might obscure the light scattering of the NCPs. The DLS plate wells were also evacuated of dust with compressed air before sample loading. The loaded plate was subsequently centrifuged for 1 minute at 4,680 rpm to settle the samples onto the bottom of the wells.

DLS autocorrelation functions were recorded using a plate reader format Wyatt DynaPro DLS instrument with a 150° detector angle and 824 nm laser irradiation and numerically fitted using the cumulants method (22, 23) to obtain z-average diffusion constants (D_z), as previously described (24). The fitted autocorrelation functions were taken as the average of 25 transients measured for an acquisition time of 1 second each, at 25 °C. In cases where artifactual transients with noisy

baselines and non-single exponential behavior were observed (deriving from residual dust or bubbles), these were manually filtered from the dataset. Effective hydrodynamic radii, R_h (Fig. 6A), were calculated from the fitted D_z values according to the Stokes-Einstein relationship $R_h = \frac{k_B T}{6\pi\eta D_z}$, where $k_B$is the Boltzmann constant, T is the absolute temperature, and η is the solution viscosity.

Fitting of DLS profiles for nucleosome self-association

The NCP DLS profiles were fit with an isodesmic model of self-association (25, 26) where it is assumed that the NCPs stack into linear assemblies (Fig. 6). In this case, a single association constant, K_A, describes each addition of an NCP monomer to a growing assembly

$$K_A = \frac{[N_2]}{[N_1]^2} = \frac{[N_3]}{[N_2][N_1]} = \cdots = \frac{[N_i]}{[N_{i-1}][N_1]} = \cdots = \frac{[N_n]}{[N_{n-1}][N_1]} \quad [3]$$

where NCP monomers are denoted by N_1, and n is the final assumed assembly size (values of 100, 200, or 300 were used in the fits with no difference in the extracted parameters). Note that NCPs can both associate and dissociate from either end of each growing assembly; that is, there are two ways to add an NCP monomer to an assembly and two ways to dissociate an NCP monomer from an assembly, meaning that this multiplicity need not be considered in the definition of K_A. As all steps are equivalent, it can be shown that

$$[N_i] = {K_A}^{i-1}[N_1]^i. \quad [4]$$

The total concentration of NCP monomers, N_T, is given by

$$N_T = \sum_{i=1}^{\infty} i[N_i], \quad [5]$$

where the stoichiometric factor *i* reflects the total number of NCP monomers in a given assembly. Here it is assumed that NCP monomers (i=1) can polymerize into infinitely long oligomers (i=∞), as this results in a useful approximation, as shown below. Substitution of Eq. [4] into Eq. [5] yields

$$N_T = \sum_{i=1}^{\infty} i K_A^{i-1}[N_1]^i. \quad [6]$$

To provide numerical stability in the fitting process, Eq. [6] can be recast using dimensionless values for the total amount of NCP monomer (X_T) and free NCP monomer (X_1), as performed previously (25, 26), using the definitions

$$X_T = K_A N_T, \quad [7]$$

and

$$X_1 = K_A[N_1]. \quad [8]$$

Finally, Eqs. [7] and [8] can be substituted into Eq. [6], yielding the dimensionless expression

$$X_T = \sum_{i=1}^{\infty} i X_1^i \quad [9]$$

and since $\sum_{i=1}^{\infty} i x^i = \frac{x}{(x-1)^2}$ when $|x| < 1$ (25, 26), it follows that

$$X_T = \frac{X_1}{(X_1-1)^2}. \quad [10]$$

The condition $|X_1|<1$ was verified in fits of each NCP DLS profile. The molar concentrations of all NCP species can be calculated upon solving for X_1 assuming a value for K_A, as was performed in the fitting procedure outlined subsequently.

D_z values were computed as the weighted average of the diffusion constants for each species (27)

$$D_z = \sum_{i=1}^{n} I_i D_i \quad [11]$$

where D_i is the diffusion constant under ideal conditions (*i.e.* infinitely dilute concentrations) of the i^{th} diffusing species, and I_i is its relative light scattering intensity, calculated as

$$I_i = \frac{m_i^2[N_i]}{\sum_{i=1}^{n} m_i^2[N_i]} \quad [12]$$

where m_i is a scaling factor equal to the ratio of the molecular weight of species *i* to that of the monomer NCP (for N_1, $m_1 = 1$, for N_2, $m_2 = 2$, etc.). Thus, Eq. [12] can be written as

$$D_z = \frac{\sum_{i=1}^{n} m_i^2[N_i]D_i}{\sum_{i=1}^{n} m_i^2[N_i]}. \quad [13]$$

To constrain the DLS fits, we used a scaling law that has previously been applied in calculating diffusion constants of higher-order oligomers for self-assembling proteins and other molecules (27, 28). The D_i values for $i>1$ are obtained by assuming that the diffusion constants for the NCP assemblies obey

$$D_i \propto D_1 i^s \quad [14]$$

where *s* is a scaling constant that takes into account the shape of the NCP particles. The scaling relationship employed here assumes that the NCP monomer and higher order assemblies behave as rods so that (29, 30)

$$D_i = \frac{k_B T}{6\pi\eta L_i}\left(2ln(\rho_i) + \nu(\rho_i)\right) \quad [15]$$

where L_i is the length of the rod, ρ_i is its axial ratio (= L_i/d_1, d_1 is the diameter of the monomer NCP and is equivalent to the rod diameter; we used the relation $\rho_i = i\rho_1 = (1/2)i$ based on the dimensions of the monomer), and ν is a second order polynomial that corrects for rod "end effects" ($=0.632+1.165\rho_i^{-1}+0.1\rho_i^{-2}$) (30). The ratio of D_i and D_1 then becomes

$$D_i = D_1 \frac{L_1}{L_i}\frac{\left(2ln(\rho_i)+\nu(\rho_i)\right)}{\left(2ln(\rho_1)+\nu(\rho_1)\right)}. \quad [16]$$

As an NCP rod is composed of *i* monomer units each with a height given by L_1,

$$D_i = D_1 i^{-1} f \quad [17]$$

where $f = \frac{\left(2ln(\rho_i)+\nu(\rho_i)\right)}{\left(2ln(\rho_1)+\nu(\rho_1)\right)}$. Fits of the DLS profiles were achieved by implementing Eqs. [3]-[13] and [17] in a minimization of the residual sum-of-squares (*RSS*) between the experimental and modelled D_z values, as previously described (24), to obtain optimal values of D_1 and K_A for each type of NCP sample. Estimates of the errors in the fitted parameters were obtained through Monte-Carlo analyses (31) and are reported in Figure 6 at the 95% confidence interval.

Supplementary Figures

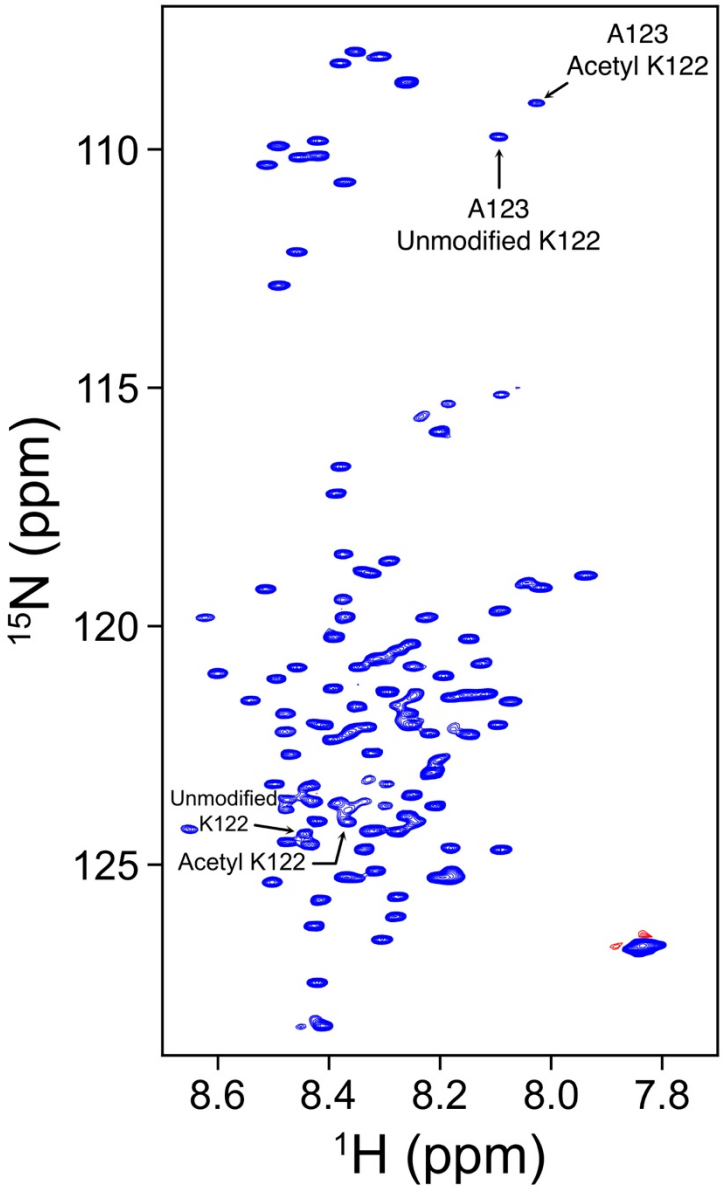

Fig. S1. ^{1}H-^{15}N HSQC spectrum of acetylated H2A in denaturing buffer. NMR spectra were recorded on a ^{1}H, ^{13}C, ^{15}N-labeled acetylated H2A sample in denaturing buffer (6 M urea, 25 mM MES, pH 5.5) to quantify the extent of acetylation of each lysine residue in this histone (similar experiments were recorded for the other histones as well). The HSQC spectrum highlighting K122 and A123 is indicated, recorded at 18.8 T, 37 ^{o}C. Backbone assignments were performed as described in Materials and Methods. Assigned peaks were classified into two categories: unmodified and acetylated, based on their sidechain ^{13}C chemical shifts, with $^{13}C_{\delta}$ chemical shifts showing the largest chemical shift perturbations upon acetylation (32) (See Fig. 1B). Partial acetylation led to a pair of amide peaks for many lysine residues, as well as for neighbouring non-lysine residues in proximity to lysines. For example, A123 showed two peaks due to partial acetylation of K122.

A

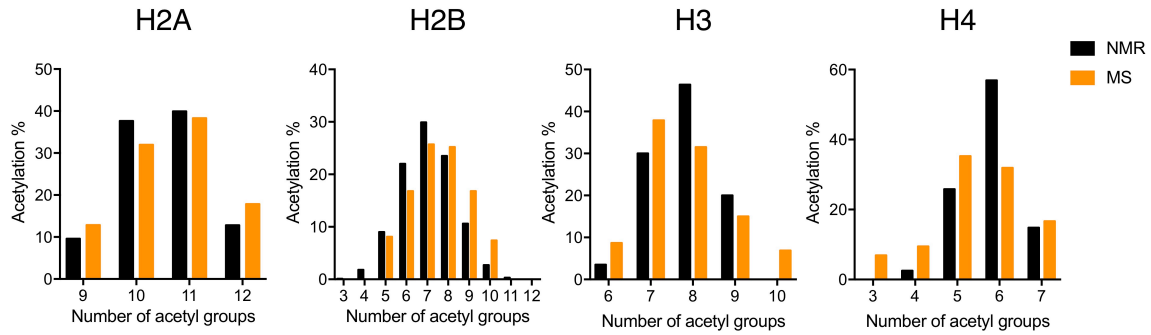

B

Lysine	% acetylated
5	100
8	100
10	100
12	100
14	100
35	100
73	100
74	71
94	0
117	42
118	100
121	100
122	43

Lysine	% acetylated
3	22
7	100
10	67
11	100
14	100
17	48
21	67
24	0
25	0
26	0
27	0
29	0
31	0
40	0
43	0
54	45
82	9
105	0
113	42
117	87
122	21

Lysine	% acetylated
4	100
9	100
14	100
18	100
23	100
27	100
36	87
37	0
56	0
64	0
79	0
115	47
122	49

Lysine	% acetylated
5	100
8	100
12	100
16	88
20	100
31	73
44	23
59	0
77	0
79	0
91	0

Fig. S2. Quantification and identification of acetyl groups in histones by NMR and mass spectrometry. (A) Distribution plots comparing the numbers of acetyl groups added to a given histone as quantified by NMR (black) and mass spectrometry (orange). The number of acetyl groups added was calculated from mass spectrometry data according to $(M_{acetyl} - M_{unmodified})/42$, where M_{acetyl} is the mass of an acetylated histone, $M_{unmodified}$ is the mass of the corresponding unmodified histone in deconvoluted mass spectra, and 42 is the mass difference upon addition of one acetyl group. Distributions can also be calculated from the NMR data by taking into account the Lys residue specific acetylation values (see below), an example of which is provided for the case of acetylated H2A:

$$P_9 = (1 - 0.71) \times (1 - 0.42) \times (1 - 0.43)$$

$$P_{10} = 0.71 \times (1 - 0.42) \times (1 - 0.43) + (1 - 0.71) \times 0.42 \times (1 - 0.43) + (1 - 0.71) \times (1 - 0.42) \times 0.43$$

$$P_{11} = 0.71 \times 0.42 \times (1 - 0.43) + 0.71 \times (1 - 0.42) \times 0.43 + (1 - 0.71) \times 0.42 \times 0.43$$

$$P_{12} = 0.71 \times 0.42 \times 0.43$$

$$P_9 + P_{10} + P_{11} + P_{12} = 1$$

where P_x is the fraction of molecules with *x* acetyl groups. (B) Tables showing sites and degrees of acetylation quantified by NMR. % acetylation of a given residue was calculated using peak intensities derived from unmodified and acetylated Lys residues in HNCO spectra.

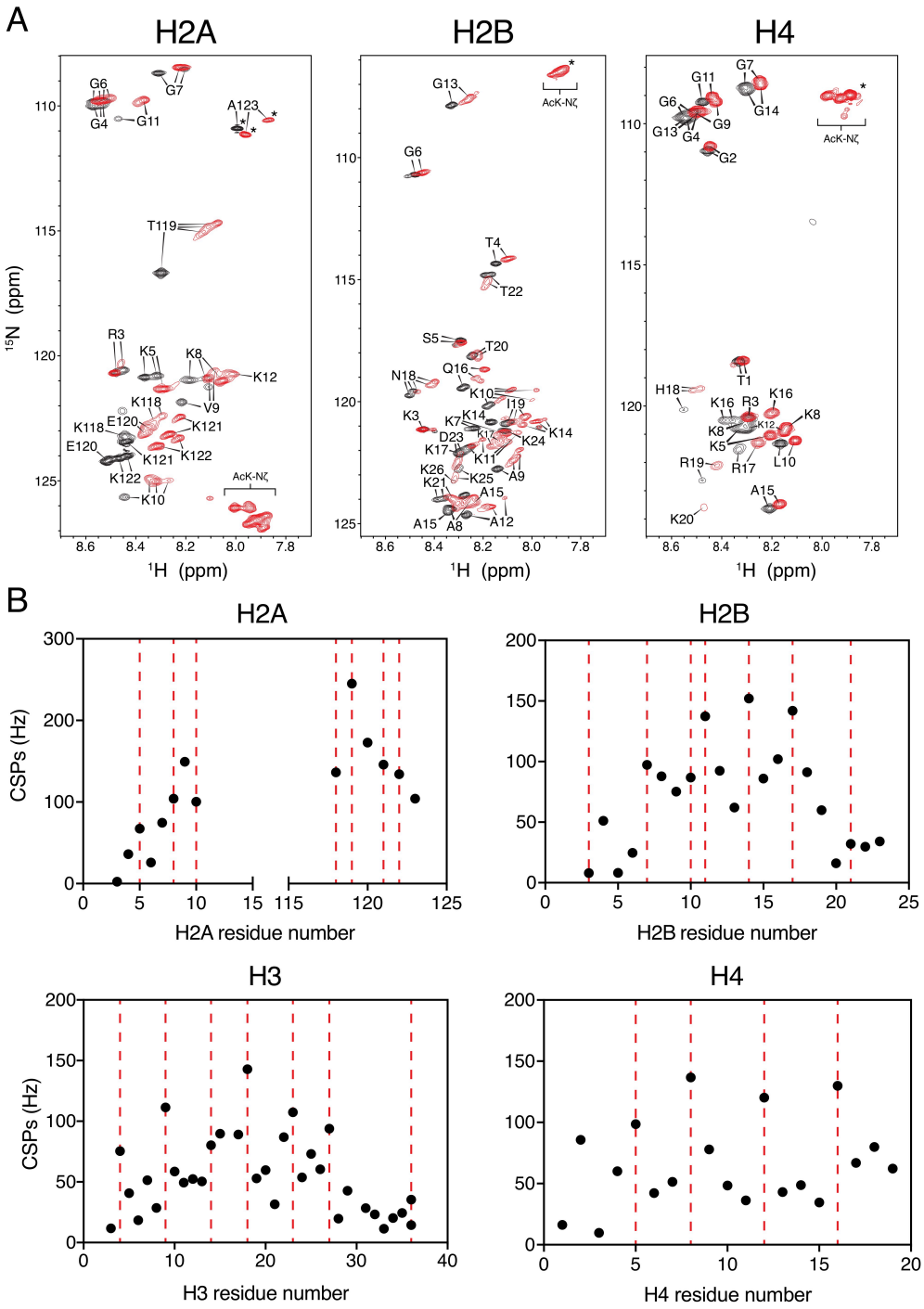

Fig. S3. Acetylation induces chemical shift perturbations (CSPs) in ^{1}H-^{15}N HSQC spectra of NCPs. (A) Overlaid amide HSQC spectra of NCPs prepared with unmodified (black, all histones unmodified, one histone ^{2}H,^{13}C,^{15}N-labeled and remaining deuterated) or acetylated (red, same histone ^{2}H,^{13}C,^{15}N-labeled as in the unmodified case but with acetylation, all other histones deuterated). Peak assignments were performed as described in Materials and Methods. All data were recorded at 37 ºC, 18.8 T. Asterisks denote aliased peaks. (B) Acetylation-induced CSPs plotted as a function of residue number. CSPs (Hz) were calculated with the following equation, $\sqrt{(\Delta\delta_H \times 800)^2 + (\Delta\delta_N \times 81)^2}$, where $\Delta\delta_i$ is the shift difference in ppm. In the case where

acetylation resulted in multiple peaks, the peak with the largest intensity was used for calculating CSPs. Dashed red lines were placed to indicate where acetylated lysine residues are located.

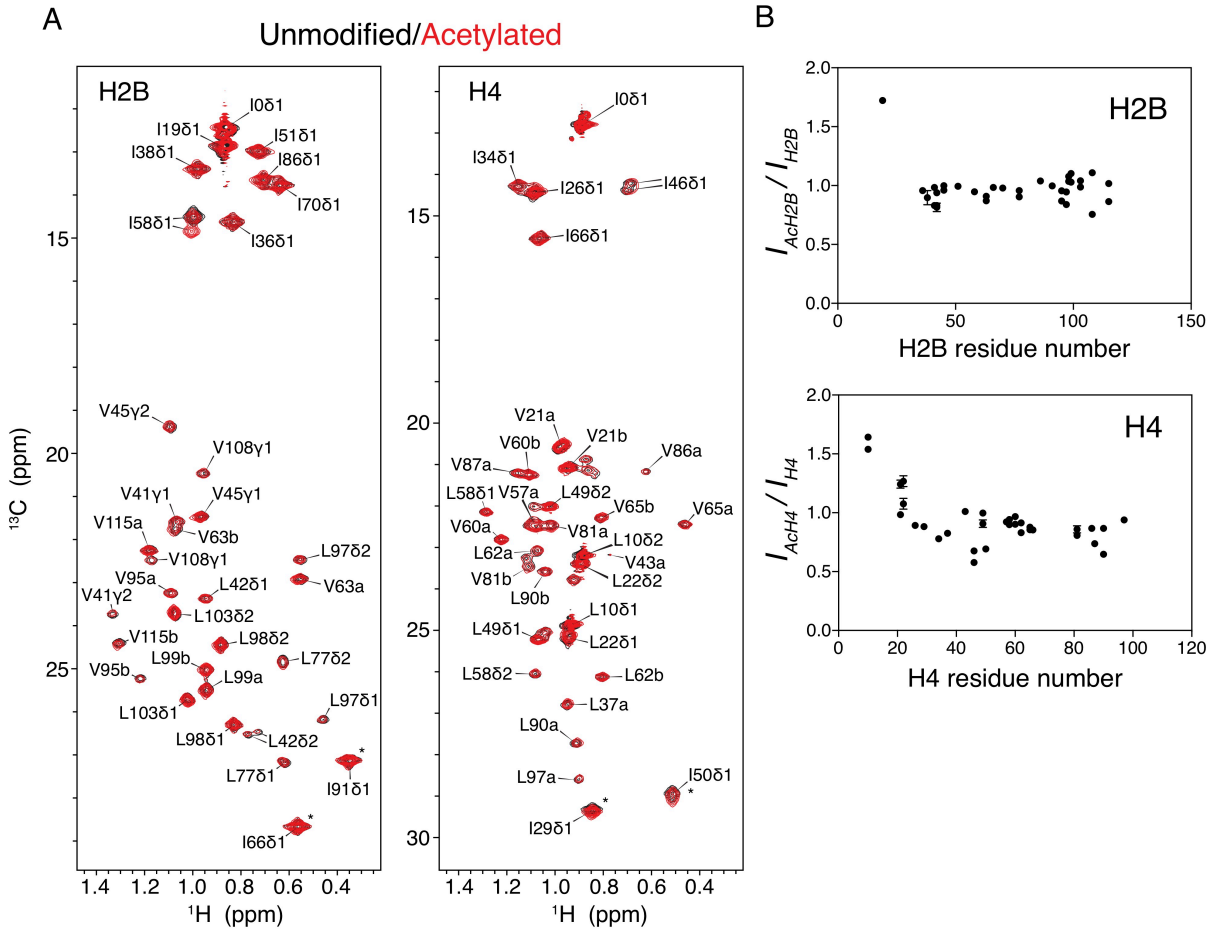

Fig. S4. Acetylation does not induce significant changes in ^{1}H-^{13}C HMQC spectra of H2B and H4. (A) Overlaid HMQC spectra of the ILV-labeled H2B (left)- and H4 (right)-NCPs reconstituted with unmodified (black) and acetylated (red) histone H2B (left) and H4 (right). Asterisks denote aliased peaks. Note that the I58δ1 (H2B) resonance is split into two peaks upon acetylation. This likely results from the fact that the sidechains of K54 and I58 are proximally positioned on the same side of helix α2 and the degree of K54 acetylation is approximately 50 % (See *SI Appendix*, Fig. S2B). (B) Intensity ratio profiles of peaks in the HMQC spectra shown in (A). The intensity ratios in the N-terminal tails (residues from 1 to 25) are generally higher than 1 due to the increased flexibility of the N-terminal tails upon acetylation.

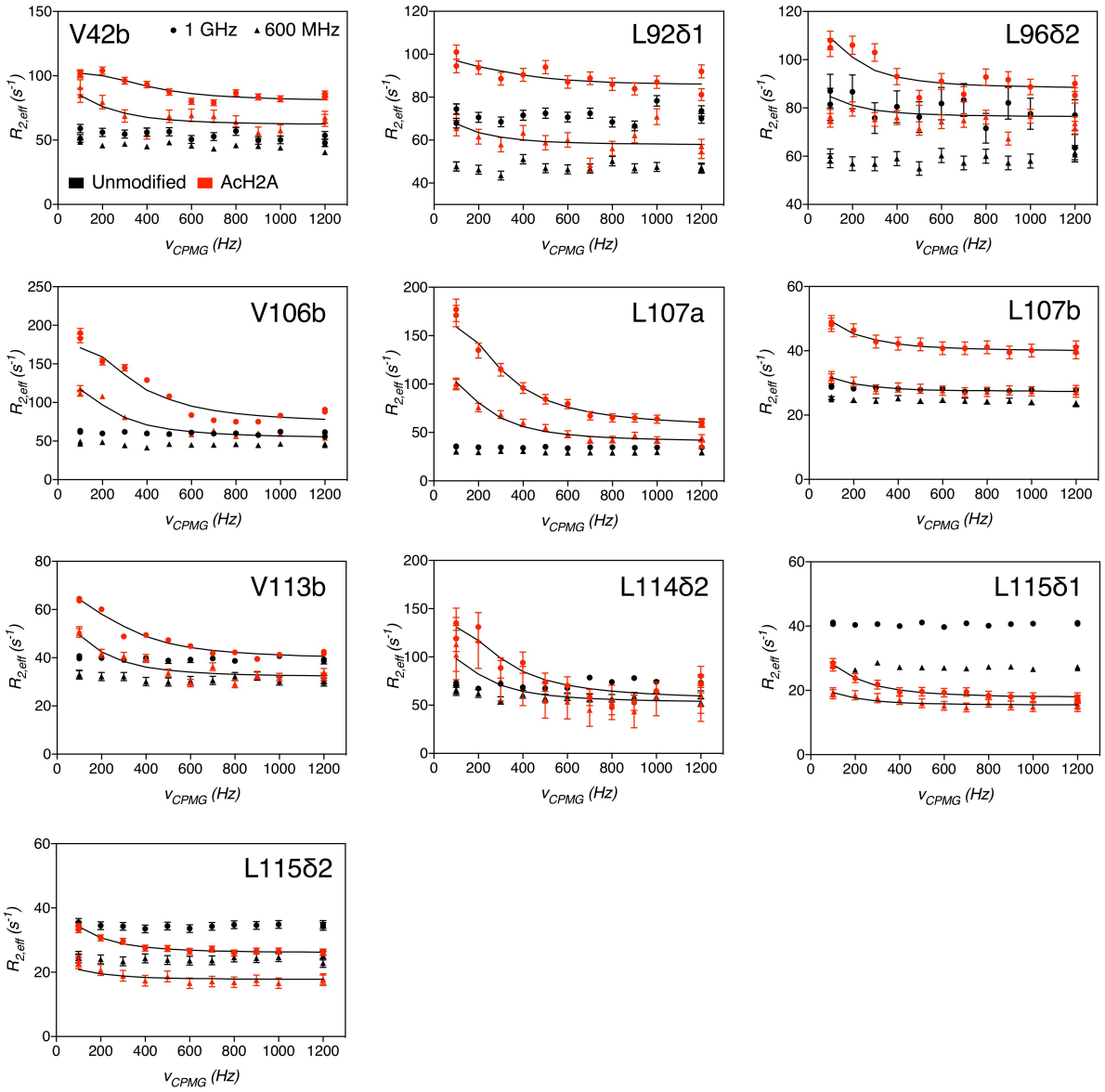

Fig. S5. ^{1}H-^{13}C multiple quantum (MQ) CPMG relaxation dispersion profiles of NCPs containing unmodified H2A (black) or acetylated H2A (red, AcH2A) histones. $R_{2,eff}$ rates (see above) were measured as a function of ν_{CPMG} at 14.1 T (triangles) and 23.5 T (circles), 37 °C. Solids lines are derived from global fits of CPMG data (*ChemEx*) using a two-state model of chemical exchange (See *SI Appendix*, Materials & Methods) to yield an exchange rate of 900±100 s^{-1} and a minor-state population of 14±1%. It is noteworthy that the $R_{2,eff}$ values for L115δ1 and L115δ2 of AcH2A at ν_{CPMG} =1200 Hz are smaller than the corresponding values in unmodified H2A. This is likely due to increased flexibility of the H2A C-terminal tail upon acetylation. Where stereospecific assignments are available they are indicated; otherwise methyl groups of Val and Leu are denoted by 'a' or 'b', as described previously (12).

A

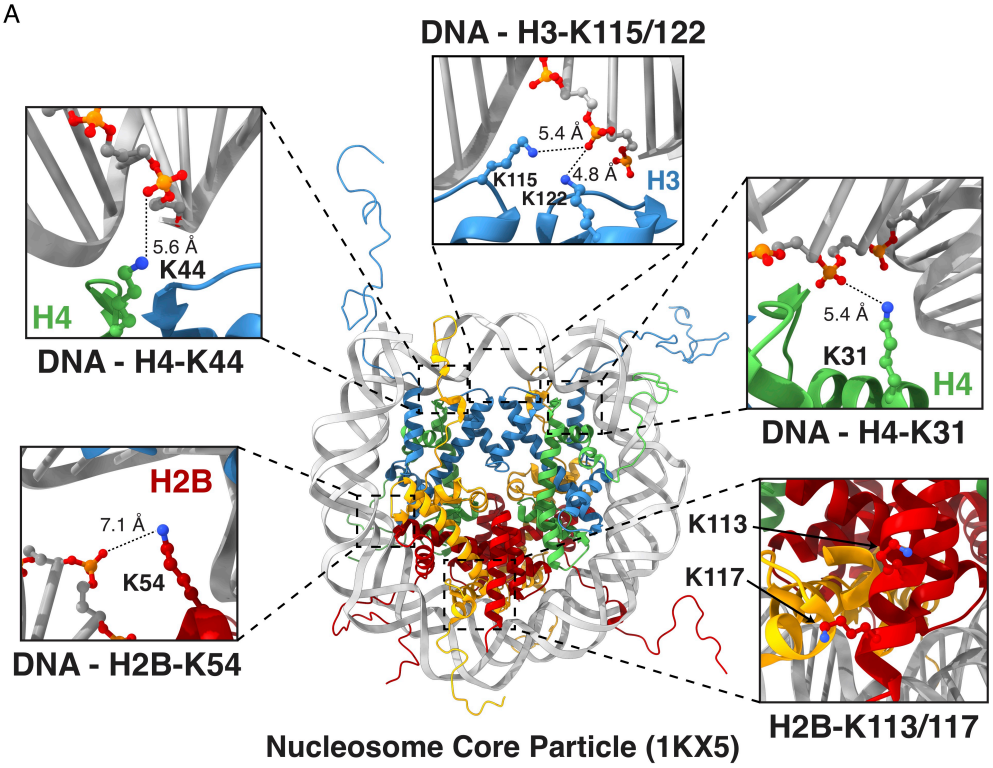

B

Histone	Residue	% acetylated	Interactions with DNA?	Distance (Å)
H2A	K35	100	Yes	6.0, 7.9, 8.1, 8.0
H2A	K73	100	Yes	7.6, 8.1, 7.2, 7.2
H2A	K74	71	Yes	3.3, 3.9, 3.7, 4.0
H2B	K40	0	Yes	4.7, 5.9, 4.7, 6.0
H2B	K43	0	Yes	6.7, 8.2, 6.3, 8.2
H2B	K54	45	Yes	7.1, 9.6, 6.7, 8.4
H2B	K82	9	Yes	7.6, 9.0, 7.6, 7.9
H2B	K105	0	No	> 12
H2B	K113	42	No	> 12
H2B	K117	87	No	> 12
H3	K56	0	Yes	4.1, 4.5, 4.8, 5.9
H3	K64	0	Yes	6.2, 7.2, 6.1, 6.6
H3	K79	0	Yes	9.3, 9.5, 10, 11
H3	K115	47	Yes	5.1, 5.8, 5.4, 6.3
H3	K122	49	Yes	4.8, 5.3, 4.8, 4.8
H4	K31	73	Yes	5.4, 7.8, 5.6, 8.0
H4	K44	23	Yes	5.3, 6.9, 5.6, 7.0
H4	K59	0	No	> 12
H4	K77	0	Yes	4.5, 5.0, 4.8, 5.0
H4	K79	0	Yes	3.1, 4.4, 2.4, 3.9
H4	K91	0	No	> 12

Fig. S6. Electrostatic interactions between nucleosomal DNA and lysine residues within the structured region of the NCP. (**A**) Structure of the NCP (1KX5 with the following color scheme: H2A, yellow; H2B, red; H3, blue; H4, green; DNA, gray) highlighting the interactions between the phosphate groups of the DNA backbone and lysine residues in the structured regions of H2B, H3, and H4. Only the residues forming contacts with DNA at distances less than 12 Å and which are acetylated more than 10% are shown. (**B**) Table summarizing the lysine residues in the structured region of the NCP, their degrees of acetylation in the samples used in this study, and their distances to the nearest region of the DNA phosphate backbone. Four distances are reported for each Lys:

these derive from the two copies of a given histone type (*i.e.*, there are two H2A K35 residues, one from each of the two H2A histones), and distances are tabulated from the Lys Nζ atom to each of the two phosphate oxygens of the DNA where the interaction occurs. Lysine residues whose sidechains are farther than 12 Å from DNA are classified as not forming interactions with DNA.

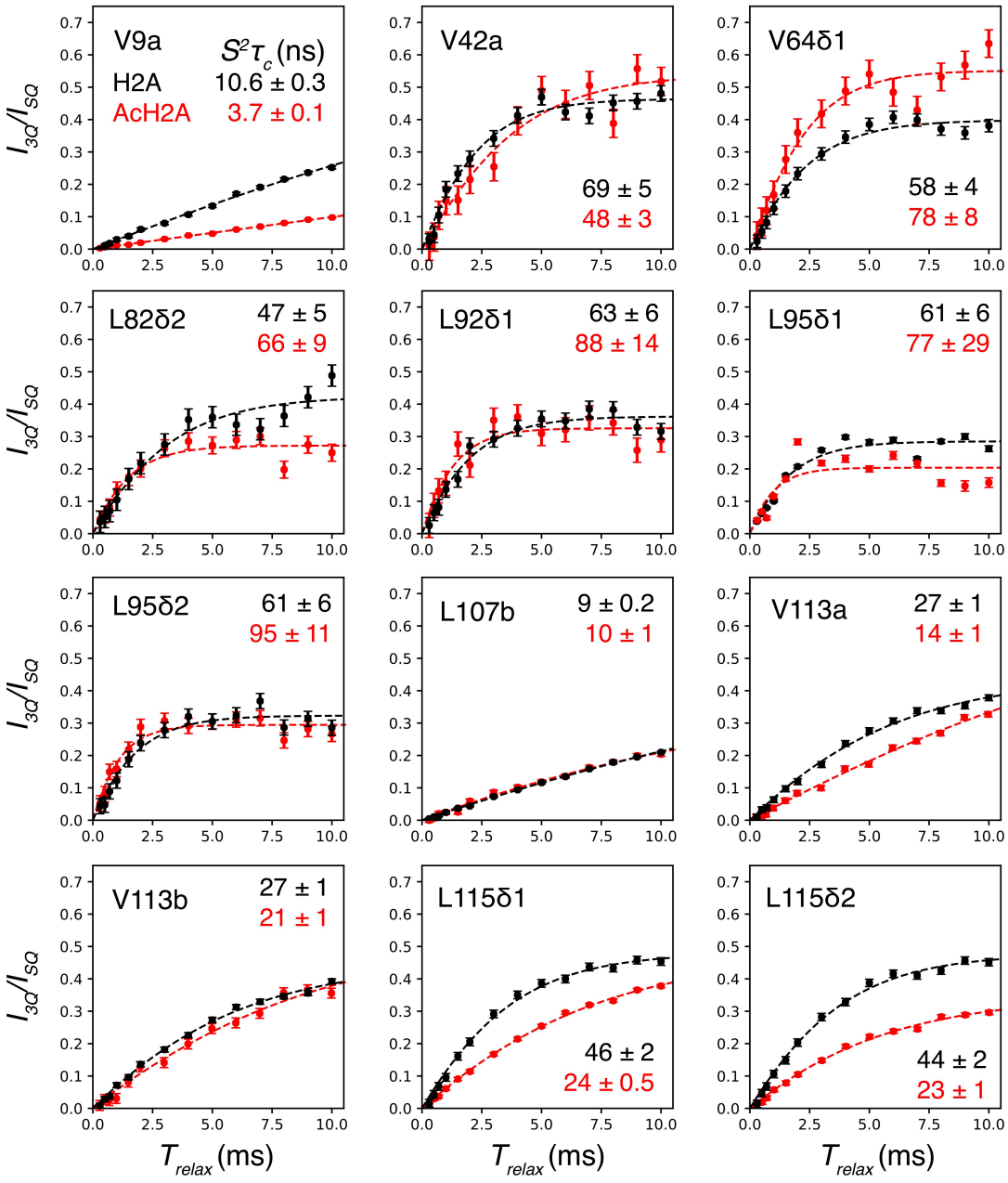

Fig. S7. Superimposed plots of I_{3Q}/I_{SQ} intensity ratios of selected methyl groups in H2A (black) and AcH2A (red) labeled nucleosomes. Ratios of differences (I_{3Q}) and sums (I_{SQ}) of single quantum methyl ^{1}H magnetization components as a function of relaxation delay, T_{relax}, measured at 14.1 T, 37 °C. Dashed lines correspond to fits obtained as described previously (19). Extracted $S^2_{axis}\,\tau_C$ values are shown in each panel. Selected residues include V9a (in the N-terminal tail) and V42a (in the L1 loop), and methyl groups that are either in the docking domain (residues 82 – 115) or interacting with it (V64δ1). Where stereospecific assignments are available they are indicated; otherwise methyl groups of Val and Leu are denoted by 'a' or 'b', as described previously (12).

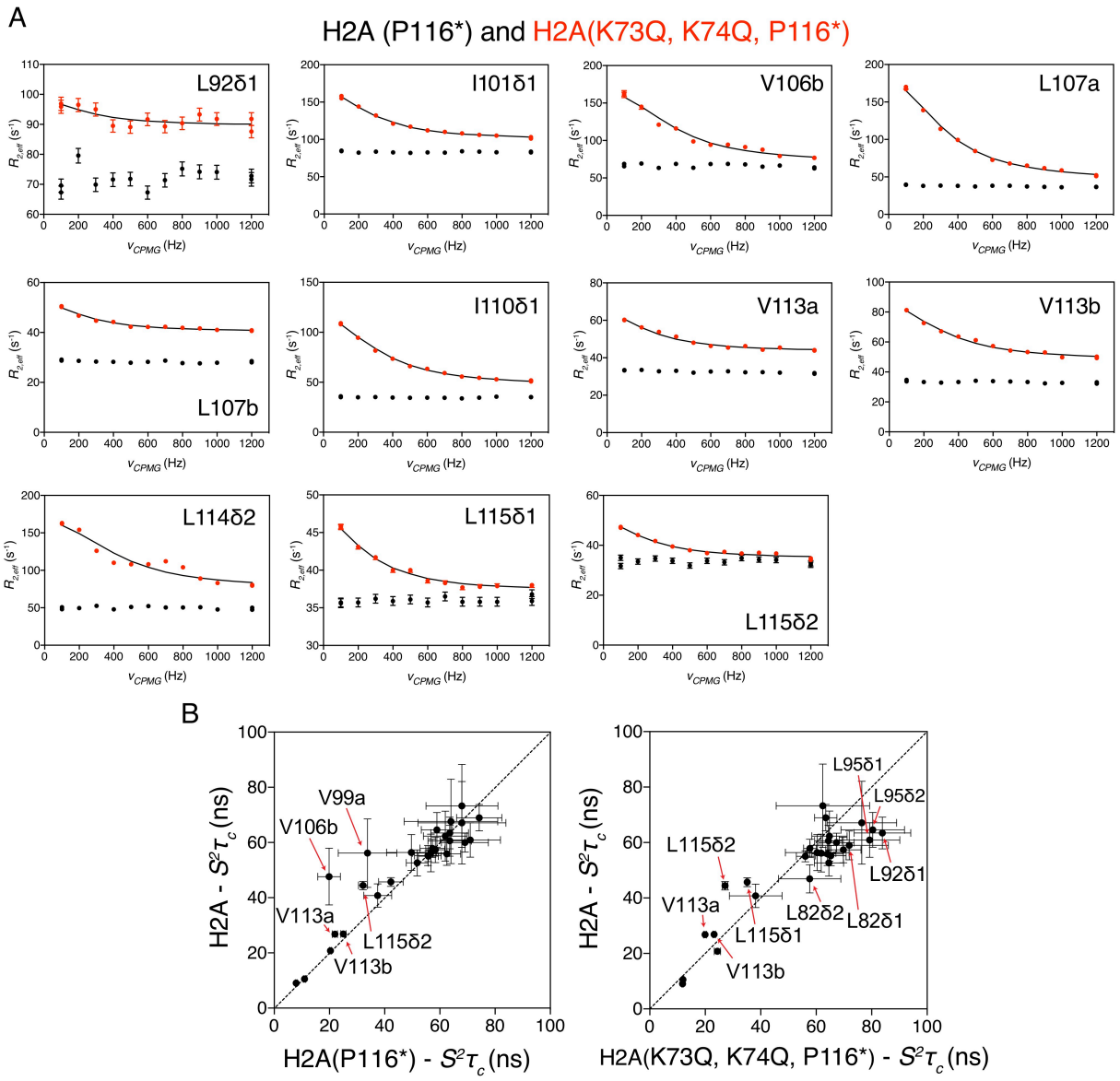

Fig. S8. Quantifying conformational dynamics of NCPs containing H2A mutants. (A) ^{1}H-^{13}C MQ CPMG relaxation dispersion profiles of NCPs containing ILV-H2A (P116*) in black and ILV-H2A (K73Q, K74Q, P116*) in red, 23.5 T, 37 °C (other three histones are NMR silent). Solid lines are global fits of datasets recorded at 14.1 T and 23.5 T using a two-state exchange model. An exchange rate of 1700±60 s^{-1} along with a population of a minor state of 16±1% were obtained for the NCP sample with H2A (K73Q, K74Q, P116*). No dynamics on the ms timescale could be observed for NCPs with H2A (P116*). (B) Correlation plots comparing $S^2_{axis}\,\tau_C$ values of NCPs with unmodified H2A or mutant H2As, (P116*) (left) or (K73Q, K74Q, P116*) (right). Dotted lines correspond to y=x to guide the eye. All data were acquired at 14.1 T, 37 °C. Where stereospecific assignments are available they are indicated; otherwise methyl groups of Val and Leu are denoted by 'a' or 'b', as described previously (12).

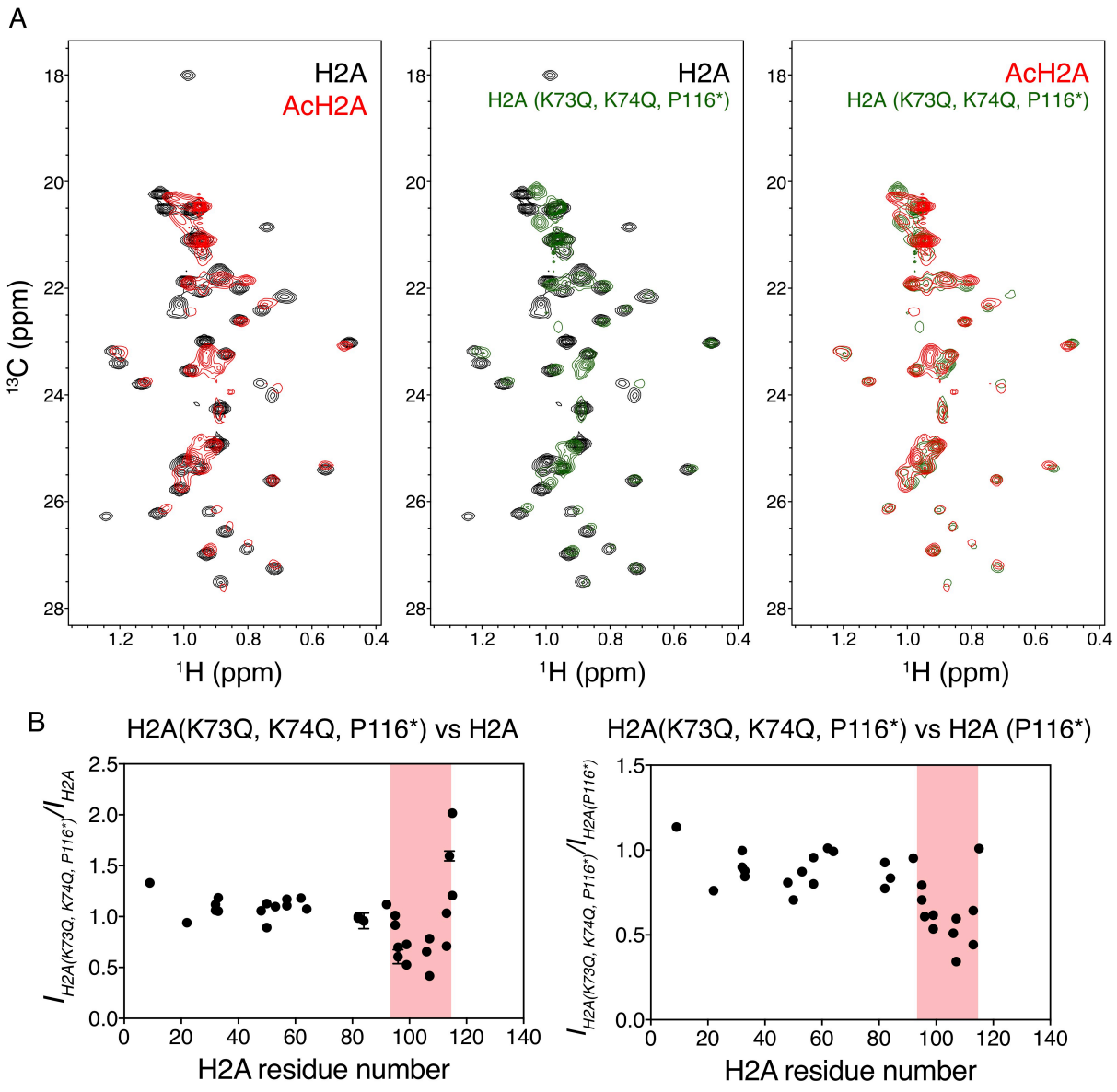

Fig. S9. NCP containing mutant H2A (K73Q, K74Q, P116*) exhibits similar conformational heterogeneity in the docking domain as the NCP with AcH2A. (A) ^{1}H-^{13}C HMQC spectra of NCPs containing unmodified H2A (black), AcH2A (red) and H2A (P116*, K73Q, K74Q) (green) acquired at 37 °C, 23.5 T (all H2A histones are ILV-labeled, with remaining histones NMR invisible). Like the HMQC spectrum of the NCP containing AcH2A, extensive peak broadening and chemical shift perturbations are present in the corresponding dataset with mutant H2A (K73Q, K74Q, P116*). Overlaid HMQC spectra of the NCPs containing AcH2A and mutant H2A (K73Q, K74Q, P116*) (right) show similarities. (B) Peak intensity ratio profiles (left; $I_{H2A(K73Q,\ K74Q,\ P116*)}/I_{H2A,}$ and right; $I_{H2A(K73Q,\ K74Q,\ P116*)}/I_{H2A(P116*)}$) plotted as a function of H2A residue number. In the left plot, the last two residues (114, 115) exhibit intensity ratios higher than 1 due to the increased flexibility following truncation of the C-terminal tail (residues from 116 to 123). The region with lower intensity ratios in the K73Q, K74Q, P116* mutant (residues from 95 to 113) is highlighted in pink.

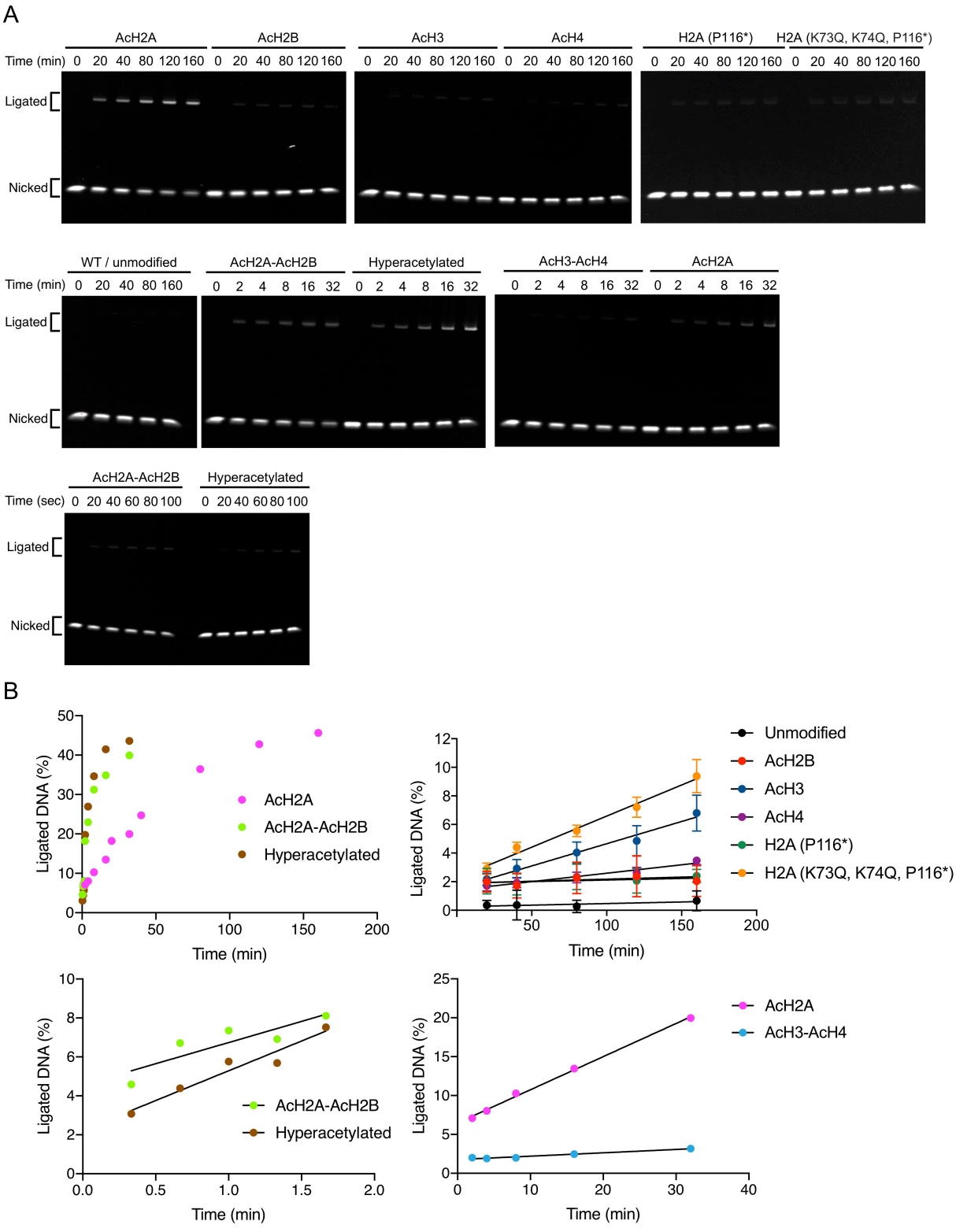

Fig. S10. Rates of ligation quantified by denaturing gels. (A) Images of denaturing DNA gels for quantifying fractions of ligated and nicked DNAs and hence ligation rates of LIG3 in the context of NCPs with histone modifications as indicated. The ligation assays were performed at 37 °C.

Fractions of ligated and nicked DNAs were measured by quantifying Alexa Fluor 647 signals. Hyperacetylated = AcH2A, AcH2B, AcH3, AcH4 in a single NCP. (B) Graphs showing fractions of ligated nucleosomal DNA ([Ligated DNA signal]/[Ligated DNA signal + nicked DNA signal]) as a function of time. Depending on the rate of ligation, different ranges of time points were used for linear regression. For the analysis of the samples with slow rates of ligation (top, right), time points from 20 to 160 minutes were used. For the analysis of the ligation reactions involving NCPs with AcH3-AcH4 or with AcH2A (bottom, right), time points from 2 to 32 minutes were used. For the analysis of the ligation reactions of NCPs containing AcH2A-AcH2B or hyperacetylated histones (bottom, left), time points from 20 to 100 seconds were used.

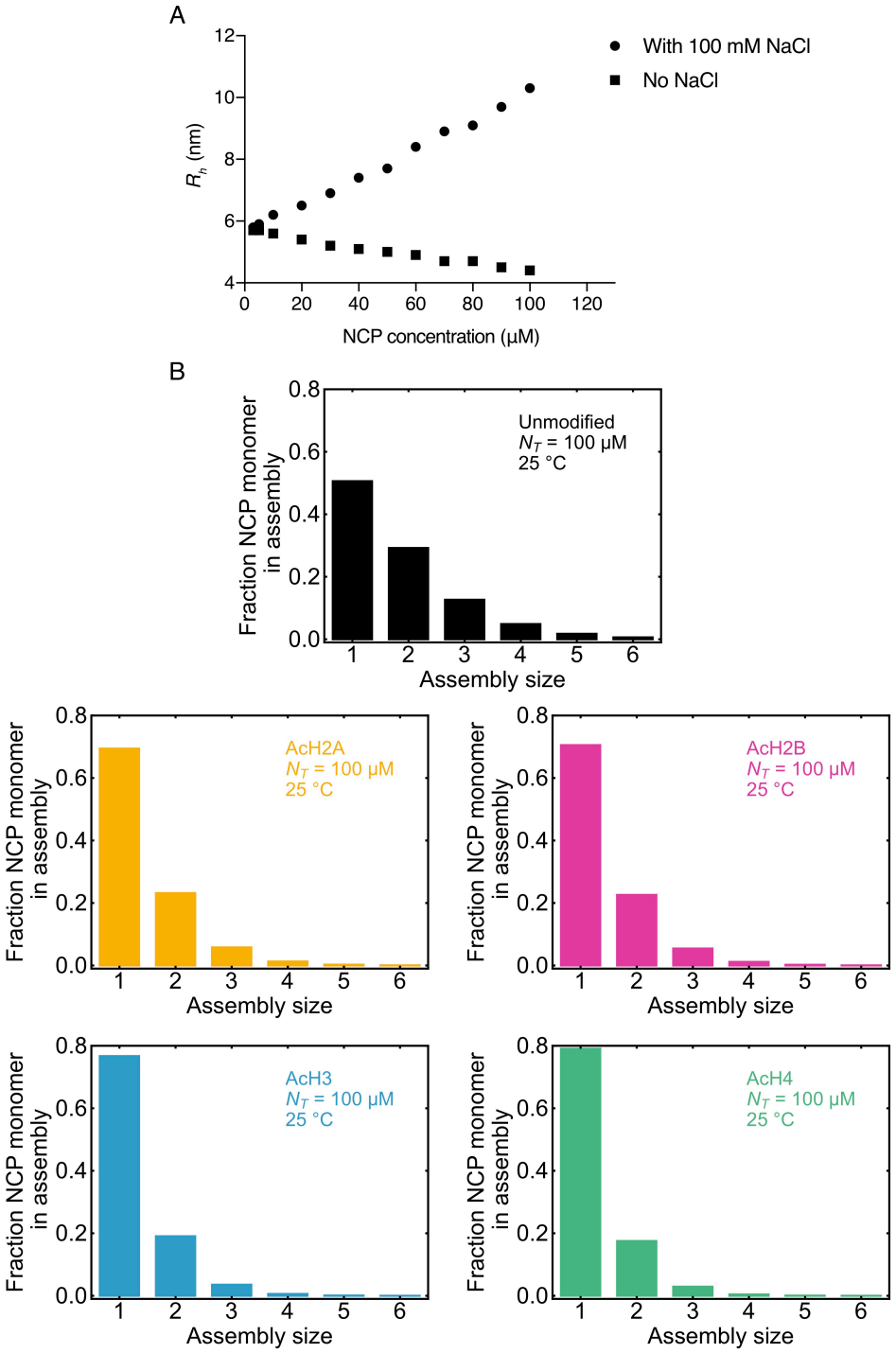

Fig. S11. Effect of NaCl on NCP diffusion and estimated oligomeric status of NCPs in the presence of 100 mM NaCl. (A) Effective hydrodynamic radii of unmodified NCPs as a function of NCP concentration as measured by DLS with/without 100 mM NaCl, 20 mM sodium phosphate, 25 °C. Note the decreasing R_h values in the absence of NaCl, corresponding to increasing diffusion constants, a nonideality condition often observed with highly charged molecules (33, 34). (B) Distributions of fractional amounts of NCP core particles populating different assembly sizes calculated from fits of DLS data using a self-assembly model. The fraction of NCP monomers in each assembly is considerably smaller than what is shown in the EM micrograph of Figure 6B. This

is due to the concentrating effect of freezing for EM so that although 100 mM NaCl NCP solutions were frozen the actual concentration of salt is likely much higher, leading to increased aggregation.

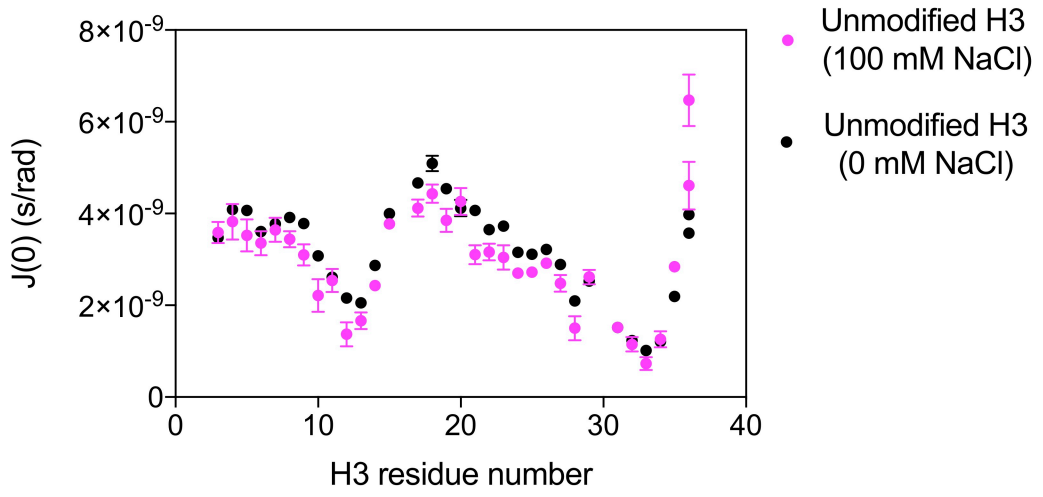

Fig. S12. Measured relaxation parameters report on intra-NCP interactions. *J*(0) values of H3 tail backbone amides in unmodified ^{2}H,^{13}C,^{15}N-labeled H3, ^{2}H-{H2A, H2B, H4} NCPs in the absence (black) and presence (magenta) of 100 mM NaCl. The experiments were performed at 37°C, 18.8 T. Addition of 100 mM NaCl increases inter-NCP interactions (Fig. 6) but does not significantly change the measured *J*(0) values. This suggests that the relaxation parameters report on intra-NCP interactions and are little influenced by transient contacts between NCPs.

SI References

1. G. Abramov, A. Velyvis, E. Rennella, L. E. Wong, L. E. Kay, A methyl-TROSY approach for NMR studies of high-molecular-weight DNA with application to the nucleosome core particle. *Proc Natl Acad Sci U S A* **117**, 12836–12846 (2020).
2. J. R. McNally, P. J. O'Brien, Kinetic analyses of single-stranded break repair by human DNA ligase III isoforms reveal biochemical differences from DNA ligase I. *Journal of Biological Chemistry* **292**, 15870–15879 (2017).
3. D.-H. Lee, *et al.*, A novel psychrophilic alkaline phosphatase from the metagenome of tidal flat sediments. *BMC Biotechnol* **15**, 1 (2015).
4. Z. Zhu, J. C. Samuelson, J. Zhou, A. Dore, S. Xu, Engineering Strand-specific DNA Nicking Enzymes from the Type IIS Restriction Endonucleases BsaI, BsmBI, and BsmAI. *J Mol Biol* **337**, 573–583 (2004).
5. J. L. Kitevski-LeBlanc, *et al.*, Investigating the Dynamics of Destabilized Nucleosomes Using Methyl-TROSY NMR. *J Am Chem Soc* **140**, 4774–4777 (2018).
6. C. R. Marr, S. Benlekbir, J. L. Rubinstein, Fabrication of carbon films with ~500 nm holes for cryo-EM with a direct detector device. *J Struct Biol* **185**, 42–47 (2014).
7. A. Punjani, J. L. Rubinstein, D. J. Fleet, M. A. Brubaker, cryoSPARC: algorithms for rapid unsupervised cryo-EM structure determination. *Nat Methods* **14**, 290–296 (2017).
8. L. E. Kay, P. Keifer, T. Saarinen, Pure Absorption Gradient Enhanced Heteronuclear Single Quantum Correlation Spectroscopy with Improved Sensitivity. *J Am Chem Soc* **114**, 10663–10665 (1992).
9. V. Sklenar, M. Piotto, R. Leppik, V. Saudek, Gradient-Tailored Water Suppression for 1H-15N HSQC Experiments Optimized to Retain Full Sensitivity. *J Magn Reson A* **102**, 241–245 (1993).
10. M. Sattler, J. Schleucher, C. Griesinger, Heteronuclear multidimensional NMR experiments for the structure determination of proteins in solution employing pulsed field gradients. *Prog Nucl Magn Reson Spectrosc* **34**, 93–158 (1999).
11. E. A. Morrison, S. Bowerman, K. L. Sylvers, J. Wereszczynski, C. A. Musselman, The conformation of the histone H3 tail inhibits association of the BPTF PHD finger with the nucleosome. *Elife* **7**, e31481 (2018).
12. H. Kato, *et al.*, Architecture of the high mobility group nucleosomal protein 2-nucleosome complex as revealed by methyl-based NMR. *Proceedings of the National Academy of Sciences* **108**, 12283–12288 (2011).
13. D. F. Hansen, *et al.*, An Exchange-Free Measure of 15N Transverse Relaxation: An NMR Spectroscopy Application to the Study of a Folding Intermediate with Pervasive Chemical Exchange. *J Am Chem Soc* **129**, 11468–11479 (2007).
14. D. F. Hansen, H. Feng, Z. Zhou, Y. Bai, L. E. Kay, Selective Characterization of Microsecond Motions in Proteins by NMR Relaxation. *J Am Chem Soc* **131**, 16257–16265 (2009).
15. N. A. Farrow, O. Zhang, A. Szabo, D. A. Torchia, L. E. Kay, Spectral density function mapping using 15N relaxation data exclusively. *J Biomol NMR* **6**, 153–162 (1995).
16. N. A. Farrow, *et al.*, Backbone Dynamics of a Free and a Phosphopeptide-Complexed Src Homology 2 Domain Studied by 15N NMR Relaxation. *Biochemistry* **33**, 5984–6003 (1994).
17. F. Ferrage, A. Piserchio, D. Cowburn, R. Ghose, On the measurement of 15N-{1H} nuclear Overhauser effects. *Journal of Magnetic Resonance* **192**, 302–313 (2008).
18. G. Lipari, A. Szabo, Model-free approach to the interpretation of nuclear magnetic resonance relaxation in macromolecules. 1. Theory and range of validity. *J Am Chem Soc* **104**, 4546–4559 (1982).
19. H. Sun, L. E. Kay, V. Tugarinov, An Optimized Relaxation-Based Coherence Transfer NMR Experiment for the Measurement of Side-Chain Order in Methyl-Protonated, Highly Deuterated Proteins. *J Phys Chem B* **115**, 14878–14884 (2011).
20. D. M. Korzhnev, K. Kloiber, V. Kanelis, V. Tugarinov, L. E. Kay, Probing Slow Dynamics in High Molecular Weight Proteins by Methyl-TROSY NMR Spectroscopy: Application to a 723-Residue Enzyme. *J Am Chem Soc* **126**, 3964–3973 (2004).

21. W. H. Press, S. A. Teukolsky, W. T. Vetterling, B. P. Flannery, *Numerical recipes in C: the art of scientific computing*, 2nd ed. (Cambridge University Press, 1992).
22. D. E. Koppel, Analysis of macromolecular polydispersity in intensity correlation spectroscopy: The method of cumulants. *J Chem Phys* **57**, 4814–4820 (1972).
23. B. J. Frisken, Revisiting the method of cumulants for the analysis of dynamic light-scattering data. *Appl Opt* **40**, 4087–4091 (2007).
24. R. W. Harkness, *et al.*, Competing stress-dependent oligomerization pathways regulate self-assembly of the periplasmic protease-chaperone DegP. *Proc Natl Acad Sci U S A* **118**, 1–11 (2021).
25. P. A. Korevaar, *et al.*, Pathway complexity in supramolecular polymerization. *Nature* **481**, 492–496 (2012).
26. D. Van Der Zwaag, *et al.*, Kinetic Analysis as a Tool to Distinguish Pathway Complexity in Molecular Assembly: An Unexpected Outcome of Structures in Competition. *J Am Chem Soc* **137**, 12677–12688 (2015).
27. A. D. Hanlon, M. I. Larkin, R. M. Reddick, Free-solution, label-free protein-protein interactions characterized by dynamic light scattering. *Biophys J* **98**, 297–304 (2010).
28. A. K. Attri, C. Fernández, A. P. Minton, Self-association of Zn-insulin at neutral pH: Investigation by concentration gradient-static and dynamic light scattering. *Biophys Chem* **148**, 23–27 (2010).
29. J. Seils, R. Pecora, Dynamics of a 2311 Base Pair Superhelical DNA in Dilute and Semidilute Solutions. *Macromolecules* **28**, 661–673 (1995).
30. M. M. Tirado, C. L. Martínez, J. G. de la Torre, Comparison of theories for the translational and rotational diffusion coefficients of rod-like macromolecules. Application to short DNA fragments. *J Chem Phys* **81**, 2047–2052 (1984).
31. D. R. Albert, Monte Carlo Uncertainty Propagation with the NIST Uncertainty Machine. *J Chem Educ* **97**, 1491–1494 (2020).
32. A. C. Conibear, K. J. Rosengren, C. F. W. Becker, H. Kaehlig, Random coil shifts of posttranslationally modified amino acids. *J Biomol NMR* **73**, 587–599 (2019).
33. B. J. Berne, R. Pecora, *Dynamic Light Scattering with Applications to Chemistry, Biology, and Physics*, Dover ed. (Dover Publications, 2000).
34. K. S. Schmitz, “Polyelectrolyte Solutions” in *Introduction to Dynamic Light Scattering by Macromolecules*, (Elsevier, 1990), pp. 205–259.